www.springer.com/41230
https://doi.org/10.1007/s41230-022-2105-z



# Effect of HEA/Al composite interlayer on microstructure and mechanical property of Ti/Mg bimetal composite by solid-liquid compound casting

**Jin Cheng[1], Jian-hua Zhao[1,2], Chun Wang[1], Jing-jing Shangguan[1,3], *Cheng Gu[1,2], and Ya-jun Wang[1]**

*1. College of Materials Science and Engineering, Chongqing University, Chongqing 400045, China*

*2. National Engineering Research Center for Magnesium Alloys, Chongqing University, Chongqing 400044, China*

*3. Beijing Power Machinery Research Institute, Beijing 100074, China*

**Abstract:** In this study, HEA/Al composite interlayer was used to fabricate Ti/Mg bimetal composites by solid-liquid compound casting process. The Al layer was prepared on the surface of TC4 alloy by hot dipping, and the FeCoNiCr HEA layer was prepared by magnetron sputtering onto the Al layer. The influence of the HEA layer thickness and pouring temperature on interface evolution was investigated based on SEM observation and thermodynamic analysis. Results indicate that the sluggish diffusion effect of HEA can effectively inhibit the interfacial diffusion between Al and Mg, which is conducive to the formation of solid solution, especially when the thickness of HEA is 800 nm. With the increase of casting temperature from 720 °C to 730 °C, 740°C, and 750 °C, α-Al(Mg), α-Al(Mg)+$Al_3Mg_2$, $Al_3Mg_2$+$Al_{12}Mg_{17}$, and $Al_{12}Mg_{17}$+δ-Mg are formed at the interface of Ti/Mg bimetal, respectively. When the thickness of the HEA layer is 800 nm and the pouring temperature is 720 °C, the bonding strength of the Ti/Mg bimetal can reach the maximum of 93.6 MPa.

**Keywords:** Ti/Mg bimetal composite; microstructure; solid-liquid compound casting; HEA/Al composite interlayer; mechanical property

**CLC numbers:** TG146.23 **Document code:** A **Article ID:** 1672-6421(2023)01-001-11

## 1 Introduction

The urgent need for environmental protection and energy conservation in industrial development makes materials with high structural integration and strong comprehensive performance gain wide attention [1-2]. Currently, various materials with different properties have been connected to meet the needs of different applications, including Ti/Mg bimetal composites which combine the excellent corrosion resistance and high temperature properties of titanium with the lightweight and recyclability of magnesium [3-5]. Combining the advantages of Ti and Mg could meet the lightweight, economic and performance requirements for the components to expand their applications in aerospace and automotive fields. Manufacturing methods of Ti/Mg bimetal composites mainly include diffusion bonding [6], friction stir welding [7-8], tungsten inert gas welding [9], laser welding [10-12], transient liquid phase bonding [13], and so on.

Compared with these methods, solid-liquid compound casting (SLCC) has the advantages of low cost and simple processing. However, restricted by the great differences in physical and chemical properties, the connection between titanium and magnesium faces many challenges [14]. Generally, adapting an interlayer between Mg and Ti is proved to be a realistic and economic approach. In our previous studies, interlayers Ni [15], Cu [16], Zn [17], Al [18] have been applied to obtain the metallurgical bonding between Mg and Ti by SLCC. Among them, Al is an important alloying element of both titanium alloy and magnesium alloy. According to the binary phase diagram of Ti-Al [19] and Mg-Al [20, 21], Al can react with Ti and Mg at a low temperature. Besides, as a low melting point metal, Al can protect the surface of the solid insert and improve the wettability of the solid-liquid interface. Xu et al. [22] revealed that $TiAl_3$ intermetallic compound layer was formed in the interface region of Ti/Mg joint with the addition of Al foil by resistance spot welding, which is the key

***Cheng Gu**

Male, born in 1990, Ph. D, Assistant Professor. His research interest mainly focuses on high strength aluminum alloy and composite materials technology, and multi-scale simulation of materials processing. To date, he has published more than 50 academic papers.

E-mail: gucheng.90@cqu.edu.cn

**Received: 2022-07-26; Accepted: 2022-08-18**

to achieve joint strengthening. Choi et al. [7] used dissimilar friction stir welding method to insert aluminum foil between titanium and magnesium. A thin intermetallic compound layer was formed at the welding interface and the joint with optimal tensile strength of 150 MPa was obtained. Zang et al. [23] also prepared Ti/Mg bimetal by laser conduction welding with Al as interlayer. The results showed that $TiAl_3$ and $Al_{12}Mg_{17}$ phase were formed at the interface between Ti and Mg, and the density of $Al_{12}Mg_{17}$ phase in the Mg fusion zone increased with the increase of Al layer thickness. At the interface of Al-coated TC4/AZ91D bimetal prepared by SLCC [18], $Ti(Al, Mg)_3$ intermetallic compound and $Al_{12}Mg_{17}$+δ-Mg eutectic structure were formed, with shear strength rising from 19.1 MPa to 48.5 MPa compared with the sample without Al interlayer. It can be seen from the above studies that the formation of intermetallic compounds through the reactions of Al interlayer with Mg and Ti is the main reason for the metallurgical bonding. However, the intermetallic compound like $Al_{12}Mg_{17}$+δ-Mg eutectic with high interfacial hardness is often the origin that the fracture occurs, which limits the further improvement of the bonding strength of Ti/Mg bimetals.

High entropy alloy (HEA) is a kind of special metal material developed in recent years, which is defined as the alloy with the concentration of each principal element being between 5at.% and 35at.% [24]. Compared with the traditional alloy materials, HEA generally exists as solid solution rather than intermetallic compound. Besides, four core effects are often used to describe HEA: high entropy effect, lattice distortion effect, sluggish diffusion effect and the 'cocktail' effect [25]. Among them, sluggish diffusion effect means the atoms in the HEA have a low diffusion coefficient. The use of HEA to achieve dissimilar metal connection has been reported [26–28]. Ding et al. [26] bonded copper and titanium by utilizing vacuum solid-state diffusion method with an interlayer of CoCrFeMnNi HEA, and solid solutions were formed at the interface. Hao et al. [27] investigated the feasibility of $(CoCrFeNi)_{100-x}Cu_x$ HEA filler metal for laser welding between TC4 titanium alloy and 304 stainless steel. The welded zone consisted of FCC solid solution and Cu-rich phase and was reliably metallurgical bonded. Using the characteristics of HEA, it is possible to impede the direct diffusion of atoms at the interface and inhibit the interlayer eutectic reaction process of Ti/Mg bimetals with Al interlayer. However, there is no report on the interface control of solid-liquid compound casting using HEA. In addition, it remains an unexplored field whether the formation of a single diffusion product between Al-Mg or a product other than the $Al_{12}Mg_{17}$+δ-Mg eutectic structure is conducive to the improvement of the binding strength of the bimetallic interface.

In this study, the HEA layer was used to hinder the diffusion of Mg atoms to Al layer and to achieve the purpose of inhibiting the eutectic reaction process at the interface of Ti/Mg bimetal composite with Al interlayer. The influences of HEA thickness and pouring temperature on interface evolution were studied in detail. Meanwhile, the mechanism of HEA/Al composite interlayer coating on the microstructure and mechanical property of Ti/Mg bimetal composites by solid-liquid compound casting was discussed.

# 2 Materials and methods

## 2.1 Material preparation

TC4 titanium alloy rod was used as the solid insert, and AZ91D magnesium alloy was the material for melting. The size of the TC4 solid insert was $\Phi$5 mm×40 mm and the mass of the AZ91D ingot was 400 g±50 g. The chemical compositions of TC4 alloy and AZ91D alloy are shown in Table 1. The composite interlayer between TC4 alloy and AZ91D alloy included a pure aluminum layer and a FeCoNiCr high entropy alloy layer. Pure aluminum (99.99%) used as Al layer material was coated on the surface of TC4 by hot-dip technology. FeCoNiCr HEA layer was deposited onto the Al layer through DC magnetron sputtering by using equimolar FeCoNiCr target. The HEA target has a radius of 25 mm and a thickness of 6 mm, which has a face-centered cubic structure demonstrated by the XRD result in Fig. 1.

Before the preparation of the composite interlayer, the surface of TC4 was mechanical ground with SiC paper and ultrasonically cleaned in degreasing solution (25 $g \cdot L^{-1}$ $Na_2CO_3$ +30 $g \cdot L^{-1}$ $Na_3PO_4$). The acid solution (50% $HNO_3$+48% HF +2% water) was used to remove the oxide film on the TC4 rod, and then, the prepared samples were placed in saturated $K_2ZrF_6$

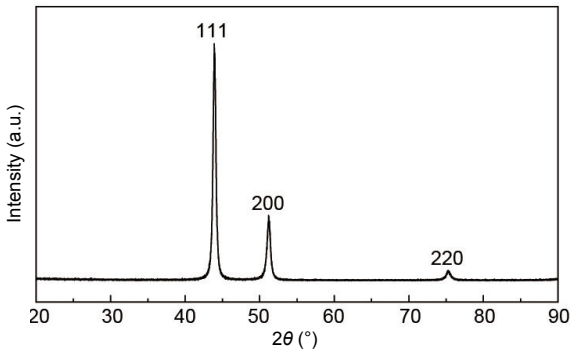


**Fig. 1: XRD pattern of FeCoNiCr high entropy alloy target material**

**Table 1: Chemical compositions of TC4 alloy and AZ91D alloy used in this study (wt.%)**

| Materials | Al | Zn | Fe | Ni | V | Ti | Mg |
|---|---|---|---|---|---|---|---|
| TC4 | 5.7–6.1 | – | 0.13–0.15 | – | 3.9–4.1 | Bal. | – |
| AZ91D | 8.7–9.0 | 0.44–0.51 | ≤0.004 | ≤0.01 | – | – | Bal. |

solution at 80 °C for 5 min to avoid oxidation before the hot-dip process. The treated samples were hot-dipped in the pure Al melt at 700 °C for 15 min, with a covering flux of about 20 mm thick. Before the magnetron sputtering of the HEA layer, hot-dip aluminized TC4 alloy was ultrasonically cleaned for 10 min to remove oil stains and impurities and then soaked in saturated NaOH solution for 60 s to remove the Al oxide film on the surface. The sputtering chamber was pumped down to $8\times10^{-4}$ Pa. The deposition of the HEA layer was carried out in 50 sccm Ar flow under the power of 100 W and pressure of 0.4 Pa. The deposition time was set as 20 min and 40 min. As shown in Fig. 2, HEA layers with different thicknesses of 400 nm and 800 nm were uniformly obtained, indicating that the selected sputtering process is reasonable.

Before solid-liquid compound casting, the mold was placed into a furnace and preheated to 300 °C. AZ91D ingots were melted in the resistance furnace and covered by the RJ-2 flux to avoid oxidation during the melting process. After the AZ91D ingots reached the predetermined temperature of 720 °C, 730 °C, 740 °C, and 750 °C, they were poured into the metal mold with solid inserts at a uniform speed, respectively. More process details are described in the authors' previous study [17].

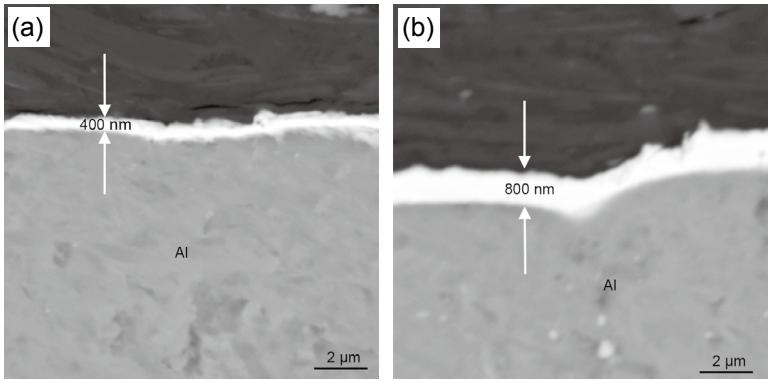


**Fig. 2: BSE images of HEA coating prepared by magnetron sputtering with different deposition times: (a) 20 min; and (b) 40 min**

## 2.2 Characterization

The interface microstructure and fracture morphology were characterized by a Tescan Vega III scanning electron microscope (SEM). The distribution of elements and the location of fracture were observed by backscattering mode (BSE). The composition distributions at the interface were analyzed by INCA Energy 350 X energy dispersive spectroscopy (EDS).

The MH-3L microhardness tester was used to measure the hardness at the interface. The working load was 100 g and the loading time was 15 s. The shear test was carried out on the WDW-100 universal testing machine. The interfacial shear strength can be calculated by the following equation:

$$\delta_\tau = \frac{F_{\max}}{\pi R h}$$

where $F_{\max}$ is the maximum load, $h$ is the height of the sample, and $R$ is the diameter of the sample. At least 3 samples were taken from each group for testing, and the results were averaged.

## 2.3 Thermodynamic calculation

A thermodynamic model was built to analyze the interface regulation mechanism. The binary formation enthalpy model was established based on Toop [29] and Miedema models [29]. The ternary thermodynamic model was established based on the modified effective thermal model proposed by Bhanumurthy [30]. The thermodynamic calculation parameters used in this study are shown in Table 2, where $T_m$ is the melting point of pure metal, $n_{ws}$ is the electrical density, $\varphi$ represents the electronegativity, $V$ represents the molar volumes of the elements, and $\mu$ is the computational constant.

**Table 2: Parameters in thermodynamic calculation [29]**

| Element | $T_m$ (K) | $n_{ws}$ (d.u.) | $\varphi$ (V) | $\mu$ | $V$ (cm$^3$) |
|---|---|---|---|---|---|
| Mg | 922 | 1.60 | 3.45 | 0.10 | 14.0 |
| Al | 933 | 2.70 | 4.20 | 0.07 | 10.0 |
| Fe | 1,812 | 5.55 | 4.93 | 0.04 | 7.1 |
| Co | 1,495 | 5.36 | 5.10 | 0.04 | 6.5 |
| Ni | 1,726 | 5.36 | 5.26 | 0.04 | 6.6 |
| Cr | 1,907 | 5.36 | 4.65 | 0.04 | 6.5 |

# 3 Results and discussion

## 3.1 Interfacial microstructure and composition

Figure 3 shows the interfacial microstructure of HEA/Al-coated TC4/AZ91D bimetal at pouring temperature of 720 °C. The corresponding EDS results of Points 1–7 in Fig. 3 are summarized in Table 3. As can be seen from Fig. 3(a), when the thickness of the HEA layer is relatively thin at 400 nm, there is a 20 μm metallurgical reaction layer at the interface between TC4 alloy and AZ91D alloy. According to EDS linear scanning results shown in Fig. 4(a), the main components of the metallurgical reaction layer are Mg and Al, and the content of Mg is higher than that of Al, indicating that the main phase at the metallurgical reaction layer is $Al_{12}Mg_{17}$ intermetallic compound. The higher magnification of Area A in Fig. 3(a) is shown in Fig. 3(b), which shows that the $Al_{12}Mg_{17}$ intermetallic compound can be observed not only in the original Al layer but also in the AZ91D matrix combined with Table 3. However, due to the hindrance of the HEA layer, the diffusion of Mg element

into the interlayer is limited, and no $Al_{12}Mg_{17}$+δ-Mg eutectic structure is generated. Some tiny needle-like phases are found at the interface [Point 2 in Fig. 3(b)], and the needle-like phases are composed of HEA elements through EDS results in Table 3. These results indicate that alloying elements in the HEA layer may diffuse into Mg melt in the process of solid-liquid compound casting. Figures 4(a) and (b) show that the main component of the HEA layer does not show obvious aggregation, and the peak value near the Al layer is larger than that of the Mg matrix, indicating that part of the elements in the HEA layer diffuse into the Al side and react with Al element. Although the thin HEA layer fails to prevent the formation of the $Al_{12}Mg_{17}$ phase, there is no $Al_{12}Mg_{17}$+δ-Mg eutectic structure at the interface, which means the HEA layer can decrease the diffusion of Mg into the Al layer.

Figure 3(c) shows the microstructure of HEA/Al-coated TC4/AZ91D bimetal when the thickness of the HEA layer is 800 nm. According to EDS line scanning results in Fig. 4(c) and Table 3, when the HEA layer is thick, the interface structure is mainly α-Al phase, and the content of the Mg element is low. The higher magnification of Area B in Fig. 3(c), as shown in Fig. 3(d), exhibits that some granular weak reaction products are generated on both sides of the HEA layer, which are proved to be α-Al(Mg) and α-Mg(Al), respectively according to the EDS results. Meanwhile, a great number of Mg elements are detected in the HEA layer [Point 5 in Fig. 3(d) and Table 3], which means that the phase constitution of the interface is α-Al(Mg)+HEA solid solution+α-Al(Mg). In addition, no needle-like phase is found near the HEA layer in Fig. 3(d), indicating that elements

**Table 3: EDS point scan results of Points 1–7 in Fig. 3**

| Point | Element (at.%) | | | | | | Phase |
|---|---|---|---|---|---|---|---|
| | Mg | Al | Fe | Co | Ni | Cr | |
| 1 | 52.20 | 47.80 | – | – | – | – | $Al_{12}Mg_{17}$ |
| 2 | 35.72 | 52.09 | 3.54 | 3.21 | 2.03 | 3.41 | Solid solution |
| 3 | 54.83 | 45.17 | – | – | – | – | $Al_{12}Mg_{17}$ |
| 4 | 84.87 | 10.06 | 1.14 | 1.36 | 1.22 | 1.35 | α-Mg(Al) |
| 5 | 43.70 | 20.11 | 8.32 | 10.33 | 7.56 | 9.98 | Solid solution |
| 6 | 7.37 | 88.00 | 1.13 | 1.10 | 1.19 | 1.21 | α-Al(Mg) |
| 7 | 2.62 | 97.38 | – | – | – | – | α-Al(Mg) |

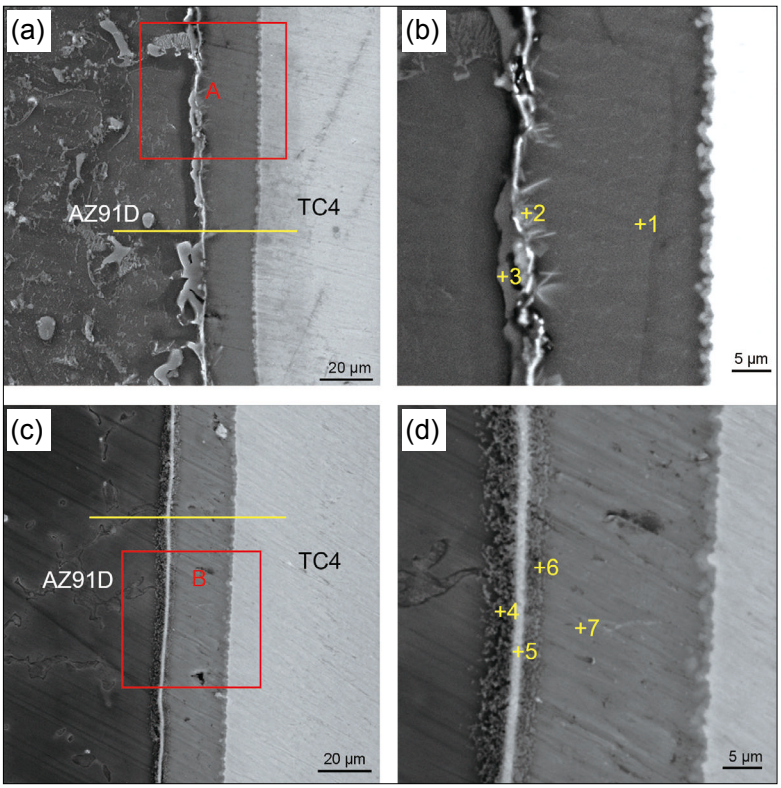


**Fig. 3: Microstructures of HEA/Al-coated TC4/AZ91D bimetal with different thickness HEA layers: (a) 400 nm; (b) high magnification of Area A in (a); (c) 800 nm; (d) high magnification of Area B in (c)**

in the 800 nm thick HEA layer do not diffuse much. It also can be seen in Fig. 4(d) that Fe, Co, Ni and Cr elements in the HEA layer form obvious element enrichment peaks near the interface, which confirms the above results.

Results mentioned above show that the HEA layer significantly inhibits the diffusion of Mg element into the Al layer and promotes the formation of a single compound interlayer during the SLCC process. To investigate the evolution of the interface, different pouring temperatures were conducted during the SLCC process. Figure 5 compares the microstructure of TC4/AZ91D bimetal with 800 nm thick HEA layer at the pouring temperature of 730 °C, 740 °C, and 750 °C. The corresponding EDS line scan results of Figs. 5(a–c) are shown in Fig. 6, and EDS results of the Points 1–9 in Figs. 5(d–f) are summarized in Table 4. According to Fig. 6(a), when the pouring temperature is 730 °C, the Mg element can diffuse across the HEA layer to the Al layer. The content of the Mg element in the Al layer decreases with the increase of the distance from the AZ91D

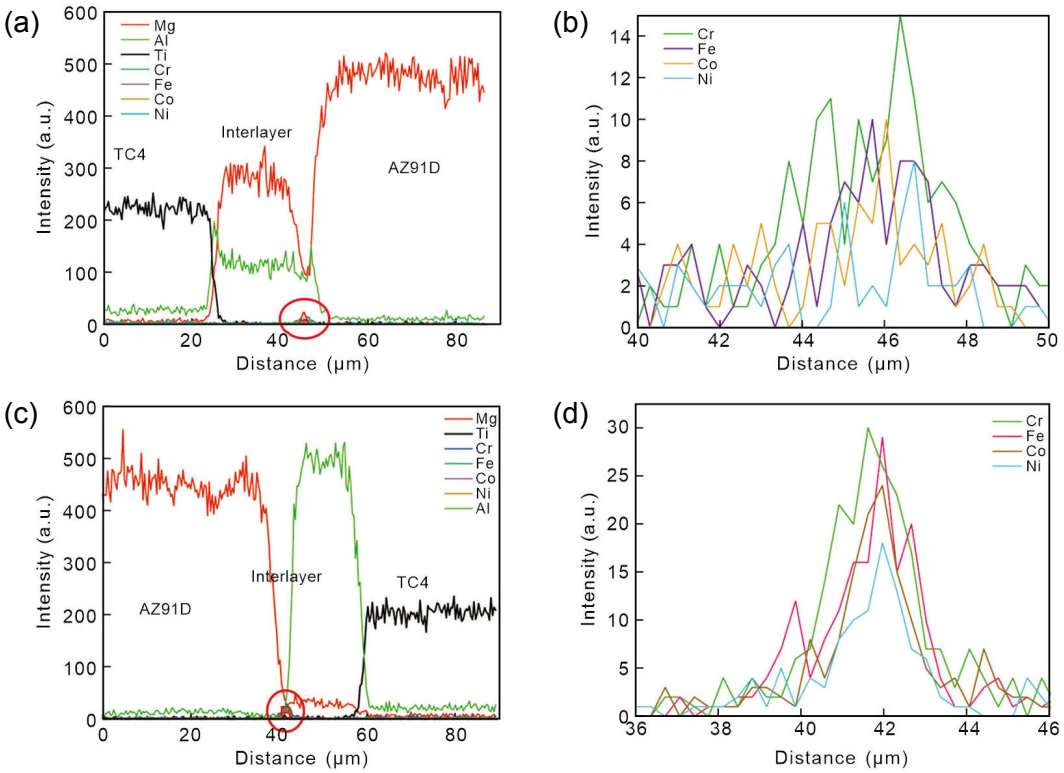


**Fig. 4: (a) EDS lines scan spectra of the yellow lines in Fig. 3(a); (b) high magnification of Area A in (a); (c) EDS lines scan spectra of the yellow lines in Fig. 3(c); and (d) high magnification of Area B in (c)**

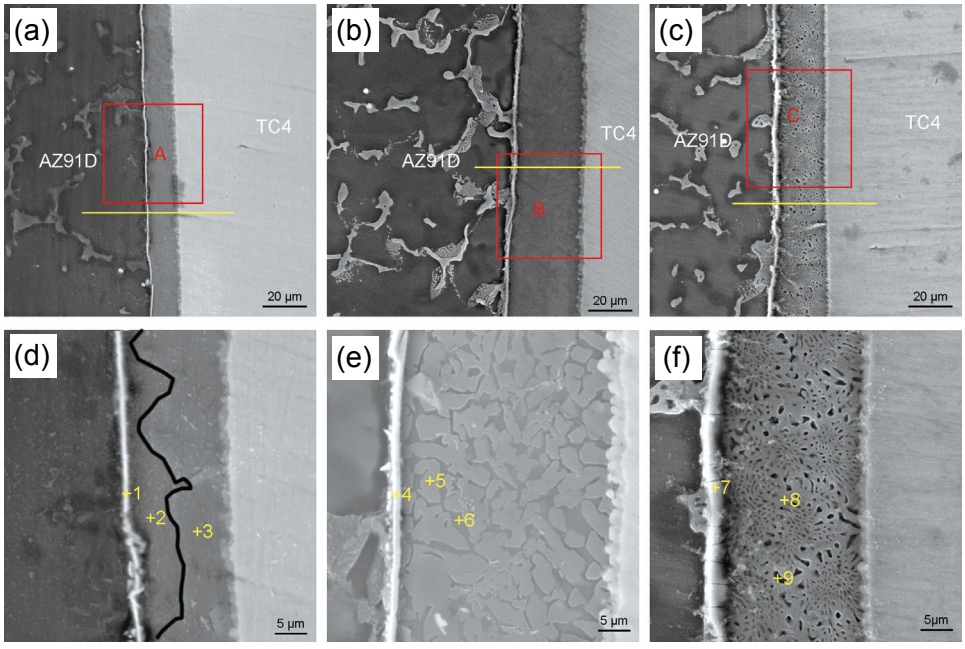


**Fig. 5: Microstructures of HEA/Al-coated TC4/AZ91D bimetal at different pouring temperatures and HEA layer is 800 nm: (a)–(c) pouring at 730 °C, 740 °C, and 750 °C, respectively; (d)–(f) higher magnification of Areas A–C in (a)–(c)**

matrix. However, the content of Mg in the Al layer is much lower than that of Al. EDS point scan results indicate that the phase near TC4 substrate (Point 3) is α-Al(Mg), while the $Al_3Mg_2$ intermetallic compound (Point 2) is formed near the HEA layer due to the diffusion of the Mg element. The boundary between the HEA layer and the Al layer is not straight, indicating that the diffusion of Mg element during the pouring process is uneven. As shown in Fig. 5(b), when the pouring temperature is 740 °C, the interface width is increased, which means that with the increase of temperature, the diffusion of Mg element into the Al layer is improved. It can be seen by the EDS results that the content of Al and Mg in the Al layer is similar. Figure 5(e) shows that there are two different phases formed at the interface. The concave phase (Point 6) contains 45.98at.% Al and 54.02at.% Mg and the convex phase (Point 5) contains 59.17at.% Al and 40.83at.% Mg. Therefore, the Al layer is composed of two intermetallic compounds, $Al_3Mg_2$ and $Al_{12}Mg_{17}$. However, as the pouring temperature increases to 750 °C, as shown in Fig. 5(c), the interface thickness decreases, and the $Al_{12}Mg_{17}$+δ-Mg eutectic structure is generated at the interface. In Fig. 5(f), cracks appear in the HEA layer. This is because a large amount of Mg diffuses into the Al layer, resulting in volume expansion. When the volume expansion exceeds the deformation limit of HEA, cracks start to nucleate.

## 3.2 Mechanical property

Figure 7 shows the microhardness distribution of HEA/Al-coated TC4/AZ91D bimetal, which exhibits great differences through the regulation of the HEA layer thickness. When the thickness of the HEA layer is 400 nm, pouring at 720 °C, the phase at the interlayer is $Al_{12}Mg_{17}$, and the average microhardness is about 300 HV. The average microhardness of all the HEA layers at 800 nm pouring at different temperatures is lower than that of the sample at 400 nm. When the interface product is α-Al(Mg) solid solution (800 nm, 720 °C), the average hardness of the interface is about 45 HV. When $Al_3Mg_2$ and Al(Mg) solid solution are formed at the interface (800 nm, 730 °C), the interface hardness distributes in a range of 50–240 HV. When $Al_3Mg_2$ and $Al_{12}Mg_{17}$ are formed at the interlayer (800 nm, 740 °C), the interface hardness is higher, reaching an average of 250 HV. With the formation of $Al_{12}Mg_{17}$+δ-Mg eutectic structure (800 nm, 750 °C), the interfacial hardness decreases to about 170 HV.

Figure 8 shows the effect of pouring temperature on the shear strength of HEA/Al-coated TC4/AZ91D bimetal. When pouring temperatures are 720 °C, 740 °C, and 750 °C, the shear curves present obvious brittle fracture characteristics. In the shear time-stress curves of 740 °C and 750 °C, the shear force fluctuates significantly as the curves rise. The shear curve of the sample at the pouring temperature of 730 °C decreases slowly after

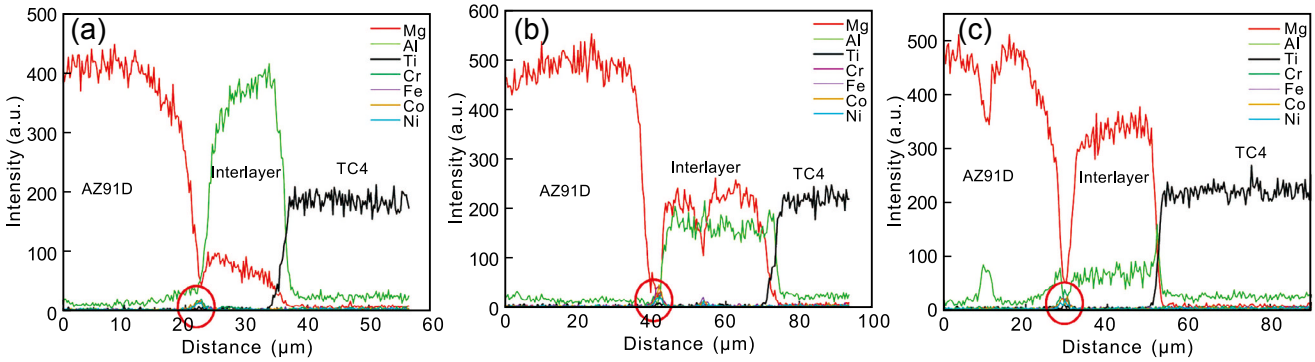


Fig. 6: EDS line scan spectra results according to the yellow lines in Fig. 5

Table 4: EDS point scan results of Points 1–9 in Fig. 5

| Point | Element (at.%) | | | | | | Phase |
|---|---|---|---|---|---|---|---|
| | Mg | Al | Fe | Co | Ni | Cr | |
| 1 | 32.48 | 12.53 | 12.04 | 16.03 | 12.50 | 14.42 | Solid solution |
| 2 | 37.84 | 62.16 | – | – | – | – | $Al_3Mg_2$ |
| 3 | 11.45 | 88.55 | – | – | – | – | α-Al(Mg) |
| 4 | 27.49 | 14.68 | 12.68 | 16.70 | 13.06 | 15.39 | Solid solution |
| 5 | 40.83 | 59.17 | – | – | – | – | $Al_3Mg_2$ |
| 6 | 54.02 | 45.98 | – | – | – | – | $Al_{12}Mg_{17}$ |
| 7 | 39.70 | 15.11 | 13.32 | 10.33 | 10.56 | 10.98 | Solid solution |
| 8 | 54.20 | 45.80 | – | – | – | – | $Al_{12}Mg_{17}$ |
| 9 | 89.95 | 10.05 | – | – | – | – | δ-Mg |

reaching the highest point, indicating that the fracture mode of the sample is accompanied by ductile fracture. It can be seen from Fig. 8(b) that the shear strength has no obvious relationship with pouring temperature, but it is related to the products formed at the interface. When the interface product is α-Al(Mg) solid solution with low hardness (800 nm, 720 °C), the shear strength is relatively high (93.6 MPa). The shear strength decreases with the formation of intermetallic compounds. When the intermetallic compound is α-Al(Mg) +$Al_3Mg_2$ (800 nm, 730 °C), the average shear strength is 73.5 MPa. When the interface product is AlMg intermetallic compound ($Al_{12}Mg_{17}$ or $Al_3Mg_2$+$Al_{12}Mg_{17}$), the shear strength is the worst, which are 28.5 MPa (400 nm, 720 °C) and 29.1 MPa (800 nm, 740 °C), respectively. With the precipitation of δ-Mg at the interface (800 nm, 750 °C), the interface hardness decreases, and the shear strength increases to 42.8 MPa.

The fracture cross-sections of the HEA/Al-coated TC4/AZ91D bimetals are shown in Fig. 9. No HEA layer is observed in Fig. 9(a) when HEA thickness is 400 nm, indicating that fracture mainly occurs in the $Al_{12}Mg_{17}$ phase when the HEA thickness is relatively thin, and the needle-like phase generated by Al and elements of HEA is observed on the interface. As the thickness of the HEA layer increases to 800 nm at the pouring temperature of 720 °C in Fig. 9(b), a relatively complete HEA layer can be observed at the fracture location, indicating that the fracture occurs at the solid solution interface between the HEA layer and the Mg matrix. In addition, cracks are found at the boundary between the Al layer and the TC4 matrix, which indicates that the bond between the Al layer and TC4 matrix also starts to be damaged. With the formation of the Al-Mg intermetallic compound, the HEA layer cannot be observed at the fracture, confirming that the shear strength of the HEA solid solution is greater than that of the Al-Mg intermetallic compound. When the interface product is $Al_3Mg_2$+α-Al, the fracture mainly occurs along the boundary between α-Al and $Al_3Mg_2$, as shown in Fig. 9(c). At this time, the fracture morphology presents tortuous, and no cracks are found between the Al layer and the TC4 matrix. When the interface products are $Al_3Mg_2$+$Al_{12}Mg_{17}$, the fracture still occurs at the boundary, as shown in Fig. 9(d). In addition, due to the great difference in hardness between $Al_3Mg_2$ and $Al_{12}Mg_{17}$, the interface even breaks under the effect of external force. As can be seen in Fig. 9(e), when $Al_{12}Mg_{17}$+δ-Mg eutectic structure is formed, the fracture mainly occurs in the eutectic structure.

Figure 10 exhibits the influence of different thickness HEA layers and pouring temperatures on the fracture morphology of TC4/AZ91D bimetal. As can be seen in Fig. 10(a), when the thickness of the HEA layer is relatively thin, the fracture is smooth and brittle fracture morphology can be observed. Part of the HEA layer and needle-like phase remain at the fracture surface. Compared with the thin HEA layer, when the thickness of the HEA increases to 800 nm and the pouring temperature is 720 °C, a great amount of residual HEA layer, as well as Mg and Al, can be observed at the fracture surface [Fig. 10(b)]. It shows that the fracture runs through the whole interface layer. Although the fracture morphology is still relatively smooth, no brittle Al-Mg intermetallic compounds can be observed. When the pouring temperature is 730 °C, the fracture morphology is no longer smooth, and many dimples are observed on the fracture surface, as shown in Fig. 10(c). The fracture is mainly composed of Al and Mg elements, indicating that the fracture of $Al_3Mg_2$+α-Al has the characteristics of ductile fracture. However, the fracture, as shown in Fig. 10(d), presents brittle fracture morphology, in which the interface product is $Al_3Mg_2$+$Al_{12}Mg_{17}$. A large number of block phases and obvious cracks are observed on the fracture surface, and the fracture is relatively smooth.

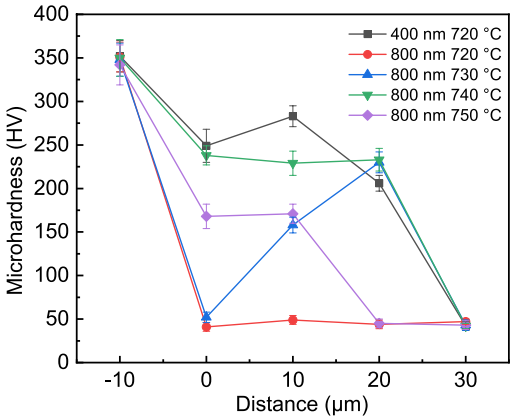


**Fig. 7: Microhardness distribution of TC4/AZ91D bimetal by solid-liquid compound casting with HEA/Al composite interlayer**

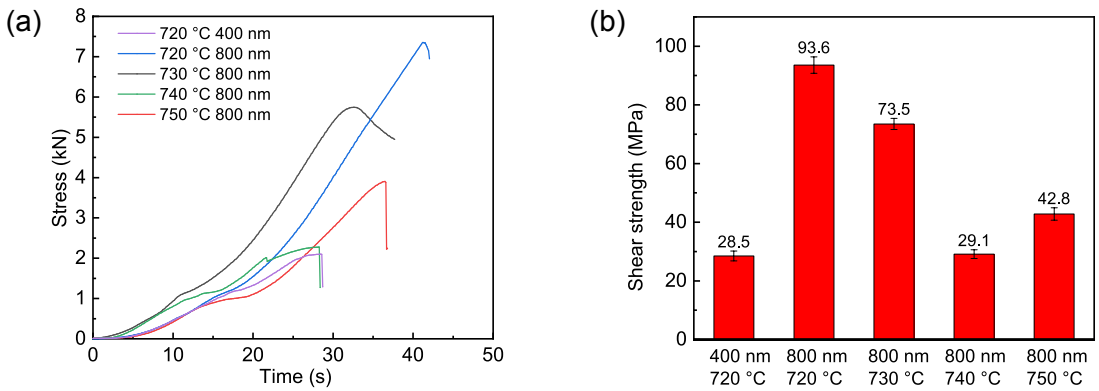


**Fig. 8: Shear strength of TC4/AZ91D bimetal by solid-liquid compound casting with HEA/Al composite interlayer: (a) time-stress curves; (b) shear strength**

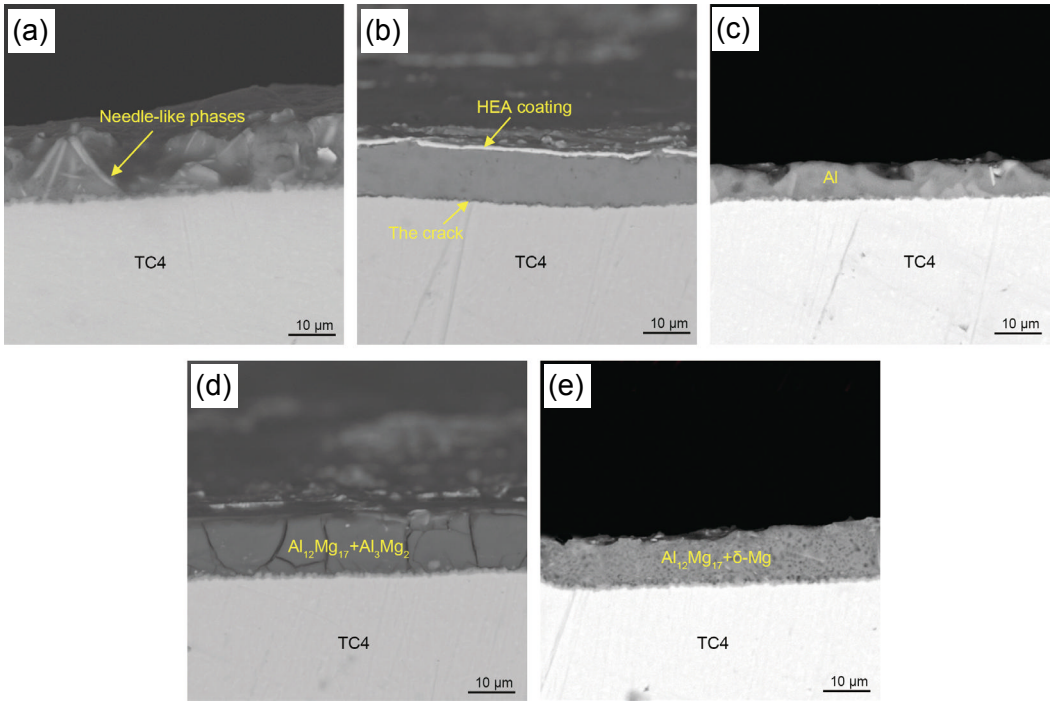


**Fig. 9: Fracture location of TC4/AZ91D bimetal by solid-liquid compound casting with HEA/Al composite interlayer: (a) thickness of HEA coating is 400 nm; (b)–(e) thickness of HEA coating is 800 nm and pouring at 720 °C, 730 °C, 740 °C, and 750 °C, respectively**

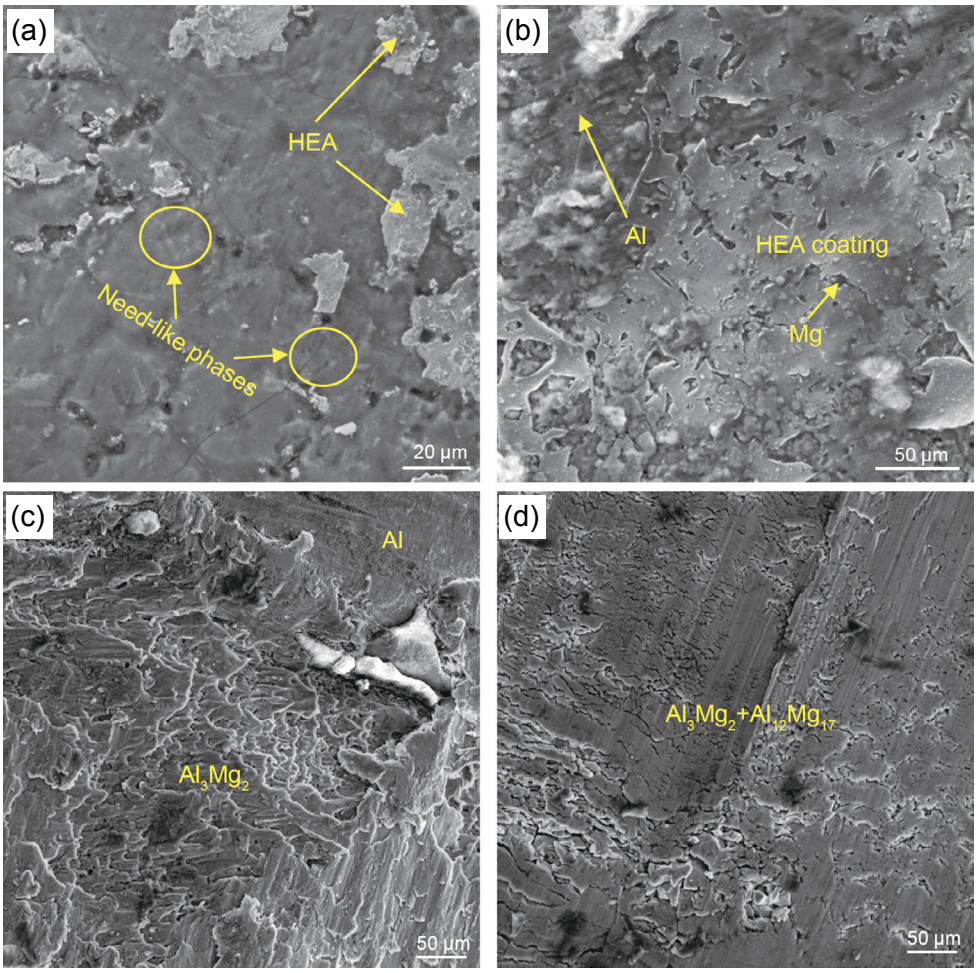


**Fig. 10: Fracture morphology of TC4/AZ91D bimetal by solid-liquid compound casting with HEA/Al composite interlayer: (a) thickness of HEA coating is 400 nm; (b)–(d) thickness of HEA coating is 800 nm and pouring temperature are 720 °C, 730 °C, and 740 °C, respectively**

### 3.3 Thermodynamic analysis and interface evolution mechanism

Under the effect of Mg melt, the elements in the thin HEA layer react with Al to form needle-like phase. As the thickness of the HEA layer increases, there are no needle-like phases formed at the interface, which can be explained by the thermodynamics of the elements. The binary formation enthalpies of Al-Fe/Ni/Cr/Co and Mg-Fe/Ni/Cr/Co were calculated, as shown in Fig. 11. It can be seen from Fig. 11(a), the binary formation enthalpies between Al and all the HEA elements are negative, which means Al can spontaneously react with all the elements of the HEA layer. It can also be determined that under the ideal condition, the first intermetallic compound generated at the interface should be Al-Cr, followed by Al-Fe, Al-Ni, and Al-Co, consequently. The formation enthalpies of Mg-Fe/Co/Cr/Ni are all positive except Mg-Ni. It indicates that Mg-Ni intermetallic compounds are most likely to be formed during the contact between the HEA layer and the Mg matrix.

Generally, under constant temperature and pressure, the system always moves in the direction of negative formation enthalpy. The lower the formation enthalpy, the easier the reaction. However, the above experiment results indicate that with the thickening of the HEA layer, the effective atomic concentration at the interface increases, but the binary phase mentioned above is no longer generated. The criterion based on ideal formation enthalpy cannot explain the interface evolution of HEA/Al-coated Ti/Mg solid-liquid compound casting. The reason may be that the interfacial reaction is usually a non-equilibrium process in the process of solid-liquid compound casting. To solve the problem that molten compounds with identical or different components may be generated simultaneously in ternary system, the co-component coefficient was introduced based on Pretorius' model [31], and the effective Gibbs free energy was modified by effective thermal model proposed by Bhanumurthy [30].

Figure 12 shows the modified calculation results of effective Gibbs free energy for the ternary systems of Al-Mg-Fe, Al-Mg-Cr, Al-Mg-Co, and Al-Mg-Ni, respectively. In any Al-Mg-*X* ternary system, the lowest Gibbs free energy is always located

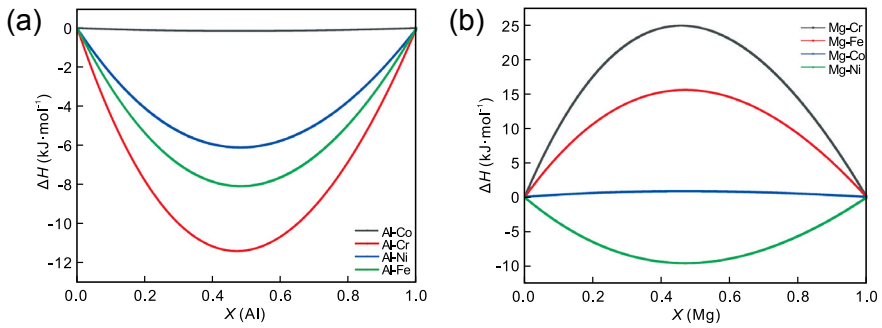


**Fig. 11: Binary formation enthalpy of Al/Mg with elements in HEA layer: (a) Al-Fe, Al-Cr, Al-Ni, and Al-Co; (b) Mg-Fe, Mg-Cr, Mg-Ni, and Mg-Co**

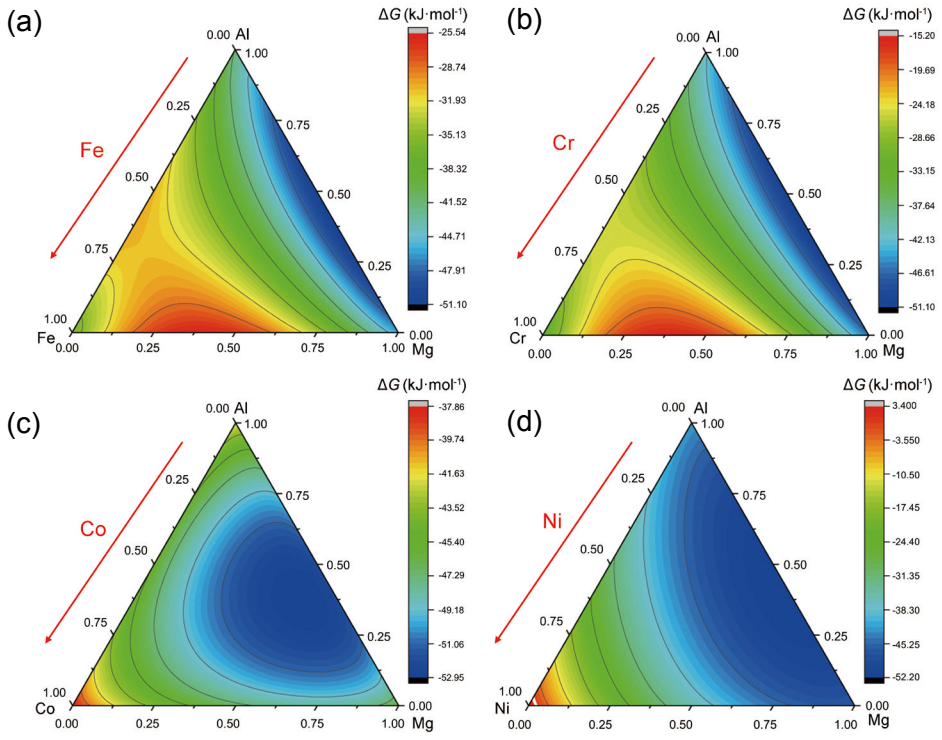


**Fig. 12: Gibbs free energy of Al-Mg-Fe (a), Al-Mg-Cr (b), Al-Mg-Co (c), and Al-Mg-Ni (d) ternary system**

on the Al-rich or Mg-rich side. If the HEA layer is relatively thin, the effective atomic concentration of Fe, Co, Ni, and Cr at the interface is low. In this case, the Gibbs free energy value of each ternary system is low, and it is possible for Al-Mg-*X* ternary phase or Al/Mg-*X* binary phase to be generated at the interface. With the increase of the HEA layer thickness, the effective concentration of the elements of the HEA layer increases. According to the thermodynamic calculation results, the overall Gibbs free energy of the ternary system increases in the direction of increasing the concentration of each element in the HEA layer (indicated by the arrow in Fig. 12). Therefore, as the thickness of the HEA layer increases, the reaction products of the HEA elements with Al or Mg are no longer formed.

Figure 13 illustrates the interface evolution mechanism of TC4/AZ91D bimetal with the HEA/Al composite interlayer. According to the above analysis results, the HEA layer with the thickness of 800 nm limits the diffusion of Mg atoms into Al layer and prevents Al atoms from spreading across the HEA to the Mg melt. The diffusion hindrance effect of the HEA layer is affected by temperature, resulting in different interface microstructures. Figure 13(a) shows the schematic of the interface diffusion during the SLCC process. At the pouring temperature of 720 °C, the content of Mg atoms diffuses into the Al layer is low (< 10at.%), and these Mg atoms dissolve into the Al layer, forming the solid solution structure with α-Al(Mg), as shown in Fig. 13(b). With the pouring temperature increases to 730 °C, the content of Mg elements in the Al layer increases to 10at.%–40at.%, and it is gradually divided into two layers. The layer near the AZ91D side contains $Al_3Mg_2$ intermetallic compound with higher Mg content, while the layer near the TC4 side is still α-Al(Mg). The final interface structure is shown in Fig. 13(c), which is mainly composed of α-Al(Mg), $Al_3Mg_2$ intermetallic compound, and HEA (Mg) solid solution. With the increase of pouring temperature to 740 °C, the content of the Mg element at the interface reaches 60at.% and exceeds that of the Al element. It can be seen in Fig. 13(d), the interface is completely composed of highly hard and brittle intermetallic compounds of $Al_3Mg_2$ and $Al_{12}Mg_{17}$. It has the highest interface hardness and the lowest shear strength, and no obvious stratification occurs. When the content of Mg element is higher than 60at.%, the eutectic reaction will occur during the cooling process, forming $Al_{12}Mg_{17}$+δ-Mg eutectic structure, as shown in Fig. 13(e).

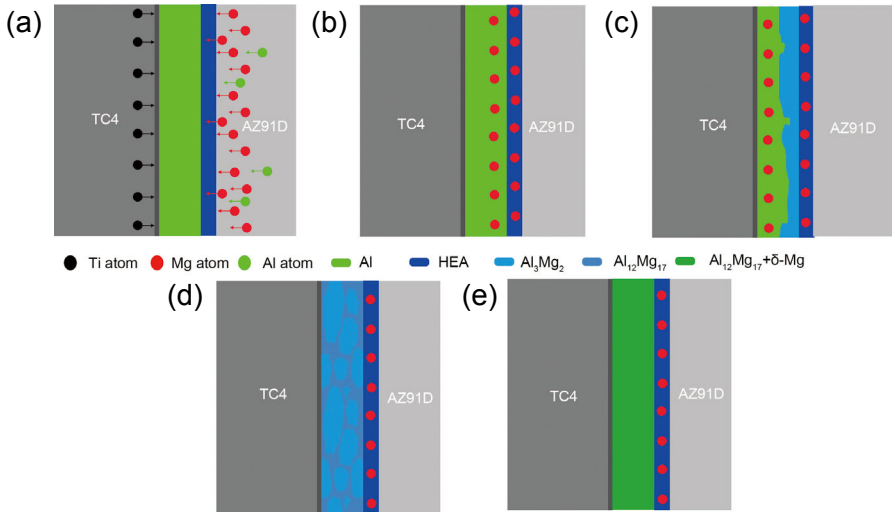


**Fig. 13: Schematic of bonding mechanism of TC4/AZ91D bimetal with a 800 nm thick HEA/Al composite interlayer (a) pouring at 720 °C (b), 730°C (c), 740°C (d), and 750°C (e), respectively**

# 4 Conclusions

In this study, the effect of HEA/Al composite interlayer on microstructure and mechanical properties of Ti/Mg bimetal composite was investigated. Ti/Mg bimetal composites were fabricated by solid-liquid compound casting process. The HEA layer was applied to control the diffusion between the Al layer and Mg matrix, and eventually improve the mechanical properties of Ti/Mg bimetal composites. The main conclusions are as follows:

(1) The HEA/Al-coated TC4/AZ91D bimetal composites were fabricated successfully by solid-liquid compound casting process. The highest shear strength of 93.6 MPa is obtained when the thickness of the HEA layer is 800 nm and the pouring temperature is 720 °C.

(2) The thickness of the HEA layer has a great influence on the microstructure formed in the interlayer. When the thickness of the HEA layer is 400 nm, the diffusion of Mg at the interlayer is limited and the $Al_{12}Mg_{17}$ intermetallic compound is formed at the interface. When the HEA layer thickness is 800 nm, the sluggish diffusion effect of HEA on the Mg element is more obvious, forming α-Al(Mg) solid solution at the interface.

(3) The diffusion hindrance effect of the HEA layer is affected by pouring temperature, resulting in different interface microstructures. The higher the pouring temperature, the more Mg elements diffuse into the Al layer. As the pouring temperature increases from 720 °C to 750 °C, the phases of α-Al(Mg), α-Al(Mg)+$Al_3Mg_2$, $Al_3Mg_2$+$Al_{12}Mg_{17}$, and $Al_{12}Mg_{17}$+δ-Mg are formed, respectively in the Al layer.

## Acknowledgements

The authors would like to acknowledge the financial supports from the National Natural Science Foundation of China (No. 51875062) and China Postdoctoral Science Foundation (No. 2021M700567).

## Conflict of interest

The authors declare that they have no conflicts of interest.

## References

[1] Li G Y, Jiang W M, Guan F, et al. Microstructure, mechanical properties and corrosion resistance of A356 aluminum/AZ91D magnesium bimetal prepared by a compound casting combined with a novel Ni-Cu composite interlayer. J. Mater. Process. Technol., 2021, 288: 116874. https://doi.org/10.1016/j.jmatprotec.2020.116874.

[2] Kota P K, Myilsamy G, Ramalingam V V. Metallurgical characterization and mechanical properties of solid-liquid compound casting of aluminum alloy: Steel bimetallic materials. Met. Mater. Int., 2022, 28: 1416–1422.

[3] Li H R, He Y Y, Zhang H C, et al. Study on the bonding mechanism of copper-low carbon steel for casting compounding process. Metals (Basel), 2021, 11: 1818. https://doi.org/10.3390/met11111818.

[4] Sistaninia M, Doostmohammadi H, Raiszadeh R. Formation mechanisms and microstructure characterization of Al/$Al_3Ni$ in-situ composite by compound casting. Metall. Mater. Trans. B, 2019, 50: 3020–3026. https://doi.org/10.1007/s11663-019-01682-1.

[5] Cooke K O, Atieh A M. Current trends in dissimilar diffusion bonding of titanium alloys to stainless steels, aluminium and magnesium. J. Manuf. Mater. Process., 2020, 4: 39. https://doi.org/10.3390/jmmp4020039.

[6] Yao F J, You G Q, Wang L, et al. Design, fabrication, microstructure, and mechanical properties of interlayer-free vacuum diffusion bonding Mg/Ti composites. Vacuum, 2022, 199: 110947. https://doi.org/10.1016/j.vacuum.2022.110947.

[7] Choi J W, Liu H, Ushioda K. Dissimilar friction stir welding of immiscible titanium and magnesium. Materialia, 2019, 7: 100389. https://doi.org/10.1016/j.mtla.2019.100389.

[8] Li Q H, Ma Z W, Ji S D, et al. Effective joining of Mg/Ti dissimilar alloys by friction stir lap welding. J. Mater. Process. Technol., 2020, 278: 116483. https://doi.org/10.1016/j.jmatprotec.2019.116483.

[9] Xu C. The study of microstructure and mechanical properties of Ti6Al4V/MB3 metallurgical joint by tungsten inert gas welding-brazing process. Mater. Res. Express., 2019, 6: 116523.

[10] Wu L, Yang J, Zang C, et al. Butt laser welding-brazing of AZ31 Mg to nickel-coated Ti-6Al-4V. J. Mater. Eng. Perform., 2019, 28: 4443–4453. https://doi.org/10.1007/s11665-019-04161-5.

[11] Tan C, Zang C, Zhao X, et al. Influence of Ni-coating thickness on laser lap welding-brazing of Mg/Ti. Opt. Laser Technol., 2018, 108: 378–391. https://doi.org/10.1016/j.optlastec.2018.07.007.

[12] Auwal S T, Ramesh S, Zhang Z, et al. Effect of copper-nickel interlayer thickness on laser welding-brazing of Mg/Ti alloy. Opt. Laser Technol., 2019, 115: 149–159.

[13] AlHazaa A, Alhoweml I, Shar M A, et al. Transient liquid phase bonding of Ti-6Al-4V and Mg-AZ31 alloys using Zn coatings. Materials (Basel), 2019, 12: 1–14. https://doi.org/10.3390/ma12050769.

[14] Baqer Y M, Ramesh S, Yusof F, et al. Challenges and advances in laser welding of dissimilar light alloys: Al/Mg, Al/Ti, and Mg/Ti alloys. Int. J. Adv. Manuf. Technol., 2018, 95: 4353–4369. https://doi.org/10.1007/s00170-017-1565-6.

[15] Wen F L, Zhao J H, Yuan M W, et al. Influence of Ni interlayer on interfacial microstructure and mechanical properties of Ti-6Al-4V/AZ91D bimetals fabricated by a solid-liquid compound casting process. J. Magnes. Alloy., 2021, 9: 1382–1395.

[16] Wen F, Zhao J, Feng K, et al. Investigation of Cu interlayer on joint formation of Ti/Mg bimetal fabricated by liquid-solid compound casting process. Met. Mater. Int., 2022, 28: 1711–1724. https://doi.org/10.1007/s12540-021-01027-1.

[17] Shangguan J J, Zhao J, Shi Y, et al. Effects of Zn interlayer on microstructures and mechanical properties of TC4/AZ91D bimetal via solid-liquid compound casting process. Int. J. Met., 2022, 16: 419–434. https://doi.org/10.1007/s40962-021-00612-9.

[18] Shangguan J J, Zhao J, Zhang J, et al. Improving shear strength of Ti/Mg bimetal composites prepared by hot-dip aluminizing and solid-liquid compound casting. Adv. Eng. Mater., 2022: 2200298. https://doi.org/10.1002/adem.202200298.

[19] Schuster J C, Palm M. Reassessment of the binary aluminum-titanium phase diagram. J. Phase Equilibria Diffus., 2006, 27: 255–277. https://doi.org/10.1361/154770306X109809.

[20] Hajjari E, Divandari M, Razavi S H, et al. Dissimilar joining of Al/Mg light metals by compound casting process. J. Mater. Sci., 2011, 46: 6491–6499. https://doi.org/10.1007/s10853-011-5595-4.

[21] Fan S, Jiang W, Li G, et al. Fabrication and microstructure evolution of Al/Mg bimetal using a near-net forming process. Mater. Manuf. Process., 2017, 32: 1391–1397. https://doi.org/10.1080/10426914.2017.1328118.

[22] Xu C, Peng C. Effect of Al interlayer on resistance spot welding of MB3/Ti6Al4V. Mater. Res. Express., 2019, 6: 1165a4. https://doi.org/10.1088/2053-1591/ab4d7a.

[23] Zang C W, Liu J, Tan C W, et al. Laser conduction welding characteristics of dissimilar metals Mg/Ti with Al interlayer. J. Manuf. Process., 2018, 32: 595–605. https://doi.org/10.1016/j.jmapro.2018.03.019.

[24] Miracle D B, Senkov O N. A critical review of high entropy alloys and related concepts. Acta Mater., 2017, 122: 448–511. https://doi.org/10.1016/j.actamat.2016.08.081.

[25] Zhang Y, Zuo T T, Tang Z, et al. Microstructures and properties of high-entropy alloys. Prog. Mater. Sci., 2014, 61: 1–93. https://doi.org/10.1016/j.pmatsci.2013.10.001.

[26] Ding W, Liu N, Fan J C, et al. Diffusion bonding of copper to titanium using CoCrFeMnNi high-entropy alloy interlayer. Intermetallics, 2021, 129: 107027. https://doi.org/10.1016/j.intermet.2020.107027.

[27] Hao X, Dong H, Xia Y, et al. Microstructure and mechanical properties of laser welded TC4 titanium alloy/304 stainless steel joint with (CoCrFeNi)100-*x*Cu high-entropy alloy interlayer. J. Alloys Compd., 2019, 803: 649–657. https://doi.org/10.1016/j.jallcom.2019.06.225.

[28] Azhari-Saray H, Sarkari-Khorrami M, Nademi-Babahadi A, et al. Dissimilar resistance spot welding of 6061-T6 aluminum alloy/St-12 carbon steel using a high entropy alloy interlayer. Intermetallics, 2020, 124: 106876. https://doi.org/10.1016/j.intermet.2020.106876.

[29] Li R Q. The application of R function to new asymmetric model and toop model. Calphad., 1989, 13: 67–70. https://doi.org/10.1016/0364-5916(89)90040-0.

[30] Bhanumurthy K, Kale G B, Garg S P. An empirical thermodynamic model to predict the first phase formation in thin film binary diffusion couples. Trans. Indian Inst. Met., 1995, 48: 193.

[31] Pretorius R, de Reus P, Vredenberg A M, et al. Use of the effective heat of formation rule for predicting phase formation sequence in AlNi systems. Mater. Lett., 1990, 9: 494–499. https://doi.org/10.1016/0167-577X(90)90094-3.